# Temporal nanofluidic confinements induce prebiotic condensation in water

**A. Greiner de Herrera**

Department of Earth and Environmental Sciences, Ludwig-Maximilians-Universität München, Theresienstraße 41, 80333 Munich, Germany. https://orcid.org/0000-0003-4257-8567

**T. Markert**

Institute of Theoretical Chemistry, Ulm University, Albert-Einstein-Allee 11, 89081 Ulm, Germany. https://orcid.org/0000-0002-2150-9442

**F. Trixler** ( Trixler@lrz.uni-muenchen.de )

Department of Earth and Environmental Sciences, Ludwig-Maximilians-Universität München, Theresienstraße 41, 80333 Munich, Germany. https://orcid.org/0000-0002-3090-4655

**Research Article**

**Keywords:** prebiotic chemistry, chemical evolution, origin of life, RNA, condensation reaction, nanofluidics, biopolymer, evolutionary conservatism, nanoconfinement, aqueous suspension

**Posted Date:** February 18th, 2021

**DOI:** https://doi.org/10.21203/rs.3.rs-163645/v3

# Abstract

A long-standing, crucial problem in the research on the chemical evolution towards the origin of life is the so-called ‘water paradox’. It states that although water is essential to life, key chemical reactions such as the synthesis of RNA are inhibited by it. Current hypotheses addressing this paradox have low prebiotic plausibility when taking the conservative nature of evolution into account. Here, we report spontaneous abiotic RNA formation in aqueous environments. The synthesis is driven by nanofluidic phenomena that alter critical properties of water. Our findings provide a solution to the paradox in a multifaceted way: abiotic, temporal nanofluidic confinements allow prebiotic condensation reaction pathways in water under stable, moderate conditions, emerge in aqueous particle suspensions as a geologically ubiquitous and thus prebiotic highly plausible environment and are consistent with the principle that evolution builds on existing pathways, as living cells also work with temporal nanoconfined water.


# Introduction

Prebiotic chemistry is facing a serious problem in regard to the role of water in abiogenesis: Although water is essential for all life as we know it, key biochemical reactions such as the polymerization of nucleotides into RNA are impeded in watery solutions[1]. In aiming to overcome this so-called ‘water problem’ in prebiotic chemistry[2], several hypotheses have been proposed[3-5]. Among them are concepts of adding condensing agents such cyanamide, using alternative solvents such as formamide, setting high temperatures of about 160°C or designing prebiotic scenarios based on wet/dry cycles. However, when appraising the plausibility of such scenarios, some general weaknesses appear[4]. First, life manages the water problem within a stable environment full of water at ambient temperatures and does not rely on conditions as proposed in such scenarios. Second, evolutionary conservatism[6] – the principle that evolution builds on existing pathways – indicates that the same physicochemical effects were involved in the abiotic origin of biopolymers, as is now being tapped by living systems via complex enzymes. Here, we demonstrate how the water paradox in prebiotic chemistry can be solved without facing these weaknesses by considering nanofluidic effects on water. According to our results, abiotic polymerizations of nucleotides into RNA can occur within aqueous dispersions of polyaromatic hydrocarbons and inorganic minerals in the absence of enzymes or additives. We present the synthesis of various amounts of RNA depending on variations of the experimental parameters and propose an explanatory model based on nonclassical effects on water when temporarily confined by suspended particles. The model describes how such nanoconfinements solve the water paradox by altering crucial physico-chemical properties of water and how evolutionary conservatism can link these natural nanofluidic reaction vessels to enzymatic biopolymerisation in biological cells.

Living cells contain an intracellular aqueous fluid that is crowded with large, complex biomolecules. In this environment, virtually all water exists as interfacial water[7]. When viewing this dense mixture from the perspective of materials science, it can be described as an aqueous suspension of highly concentrated nanoparticles. In the vicinity of such particles, various nanofluidic phenomena[8,9] emerge in interfacial

and nanoconfined water. Consequently, such water differs significantly compared to bulk water in terms of properties such as reactivity, H-bonding network dynamics, density, dielectric constant or the quantum state of protons[10-12]. From a geochemical point of view, aqueous suspensions of mineral particles of micro- and nanoscopic size can be regarded as a comparable environment that generates nanofluidic effects. Inspired by this similarity, we designed experiments to test the potential of nanofluidic environments within aqueous suspensions of particles for inducing key biochemical reactions in a possibly prebiotic context. As the abiotic synthesis of RNA in water is a common goal of prebiotic chemistry and synthetic biology[13,14], we chose the polymerisation of nucleotides into RNA as an example reaction. The focus was on the formation of a pure adenosine-based RNA (poly-A-RNA) since adenosine monophosphate (AMP) is the most common nucleotide in living cells[15]. Furthermore, poly-A-RNAs are common RNAs in cells in the form of poly-A-tails of messenger RNAs during protein biosynthesis. Thus, we first prepared samples that contained dissolved AMP. To create a nanofluidic environment for AMP solutions, we selected quinacridone (QAC) as an example of polyaromatic heterocycle particles and graphite as an inorganic suspended particle species, as both compounds have been well characterised in terms of inducing nanofluidic phenomena in aqueous suspensions[16].

# Results

### Fluorometric poly-A-RNA concentration determination.

Figure 1a shows the results of fluorometric RNA concentration measurements of such samples. Ethanol precipitation to isolate possible poly-A-RNAs of 2-10 nt length and isopropanol precipitation to isolate such RNAs longer than 10 nt were applied. The results of both precipitation methods reveal that poly-A-RNA strands have formed in significant amounts with respect to the negative controls (Fig. 1c) and that oligonucleotides of more than 10 nt length are abundant in such samples.

### RT-qPCR analysis.

To cross-check the fluorometric analysis with a totally independent but also highly specific method, we performed quantitative polymerase chain reaction after reverse transcription (RT-qPCR). The results (Fig. 2a) show that the fluorescence signal of the sample exceeds the background fluorescence after 7.57 cycles. This indicates a high yield (103-fold) of input RNA in comparison to the respective signal of the positive control miRNA (14.25 cycles). To obtain more information about the length of the formed RNA we performed a comparative melting curve analysis. This analysis included the sample RNA and a positive control miRNA with a length of 23 nt. The comparison reveals that the medium melting point of the sample is at a higher temperature than the positive control (Fig. 2b). These results suggest that the sample contains created oligonucleotides with lengths of equal to or longer than 23 nt.

### Identifying factors that determine abiotically induced polymerisation.

To identify substantial factors that lead to the observed abiotic polymerisation we first analysed the possible role of π-stacking of nucleoside monophosphates (NMPs), as stacking has been suggested to

be an important factor for RNA polymerisation in terms of bringing the monomers in close contact[17]. To perform this analysis, we extended the fluorometric analysis of ethanol precipitated AMP-based samples to CMP- and UMP-based samples and compared the relation of the different RNA concentration results with the relation of respective published stacking equilibrium constants and stacking free energies of NMPs. The comparison reveals that the detected relative concentration of poly-A-RNA is about four times higher than that of poly-C-RNA and poly-U-RNA (Fig. 1a) and that this order (poly-A-RNA >> poly-C-RNA ~ poly-U-RNA) correlates to the order of the respective stacking equilibrium constants and stacking abilities derived from the stacking free energy profiles of NMPs[18]. This correlation suggests that in particle suspensions, stacking and polymerisation of nucleotides are linked. Therefore, enhancing the stacking ability of a nucleotide should result in a higher RNA concentration. To test this hypothesis, we selected UMP due to its low self-stacking ability and its comparatively low poly-U-RNA formation and added the amino acid arginine to the sample mixture. Arginine is known for its high stacking ability with aromatic groups[19]. Fluorometric analysis of UMP/arginine-based samples revealed that arginine increased the formation of poly-U-RNA by more than 100% (Fig. 1a). This observation supports the necessity of π-stacking for polymerisation in aqueous suspensions and points to a possibly prebiotically relevant kind of interplay between amino acids and nucleic acids.

However, base stacking cannot be the key factor for RNA formation in the described samples. This becomes evident when taking the water paradox into account and when considering the result of a negative control based on an AMP solution without suspended particles (Fig. 1c): Although AMP has the highest self-stacking constant among all NMPs[18] and is the only NMP with the ability to self-associate in indefinite stacks[20], the negative control shows that in comparison to the poly-A-RNA concentrations reported above, only minute amounts can be found when the sample contains no added particles. This result suggests that there is a key factor in promoting both stacking and polymerisation that is closely linked to the particle suspension nature of the samples.

It is known that reducing the dielectric constant of water favours stacking[20], and reducing the activity of water (e.g., by adding alternative solvents or inducing wet/dry cycles) enhances polymerisation[3,21]. As nanofluidic phenomena emerging in nanoconfined water can reduce both properties simultaneously[11,22] and watery suspensions of particles give rise to such phenomena[8], we infer that the occurrence of nanofluidic phenomena in our samples is the key factor for the observed nucleotide polymerisation. This implies that the enhancement of nanofluidic effects should correlate with an increase of polymerisation reactions.

### Comparing the extent of nanofluidic effects to polymerisation efficiency.

Nanoconfining environments change the behaviour of water, especially in terms of its hydrogen bond network dynamics[11], which, in turn, affects the thermodynamic property of water activity[22]. The anomalous behaviour of nanoconfined water results from a highly complex interplay of various nanofluidic phenomena and forces that are related to, for example, the surface energy and size of the

confining boundaries, shear, molecular structure, electrical double layer and fluctuations of general order parameter[8,23]. To cope with this high complexity when assessing a possible synergy between nanofluidic phenomena and polymerisation, we chose an experimental approach that allows us to focus on a single, quantifiable effect. This approach uses the effect of organic solid/solid wetting deposition (OSWD) as a probe. OSWD is the final result of a network of various nanofluidic phenomena on confined water between suspended organic crystals, including double layer forces, Casimir-like fluctuation-induced forces and dewetting-induced hydrophobic collapse[16]. It manifests as the adsorption and self-assembly of insoluble polyaromatic heterocycles at solid/solid interfaces and thus is quantifiable via surface coverage determination.

We quantified the efficiency of OSWD as a function of different biomolecules dissolved in watery suspensions of QAC particles. For quantification, we measured the surface coverage of graphite crystals with QAC monolayers via scanning tunnelling microscopy (see Supplementary Fig. 1, Fig. 2). The results (Fig. 3) reveal that adding AMP to the particle suspension enhances the coverage with very high statistical significance ($p < 0.0001$) in relation to QAC suspensions based on pure water (w/o, Fig. 3). A significant increase in coverage ($p < 0.01$) also occurred when using arginine as the added biomolecule. By contrast, coverages found in samples based on CMP or UMP are statistically nearly identical and significantly lower with respect to the AMP- and arginine-based samples. Using a mixture of different NMPs leads to no significant increase in coverage but results in some very high single coverage measurements with respect to the CMP and UMP samples (NMPs, dot plot, Fig. 3), possibly caused by clusters of the AMP fraction of the mixture. The comparison of these OSWD-induced coverages with RNA quantities (Fig. 1a) indicates that relative differences in the extent of nanofluidic phenomena between the samples correlate with relative differences in RNA concentrations. This supports the hypothesis of a synergy between nanoconfinement effects and nucleotide polymerisation in aqueous particle suspensions. We thus propose that the emergence of nanofluidic effects on confined water is the key factor in the promotion of both stacking and polymerisation of nucleotides within aqueous suspensions of particles.

## Assessing the generalisability of suspension-induced polymerisation.

Thus far, we used QAC/graphite particle systems to ensure comparability of the results from different experimental approaches. To test whether the formation of RNA in such an environment is generalizable, we measured samples prepared by the same protocol but containing particles based on other compounds. As inorganic substitutes, we chose magnetite and silica as geologically widespread compounds and selected the organic compound anthraquinone as being abundant in carbonaceous meteorites[24]. Fluorometric measurements of partly or fully substituted samples show poly-A-RNA concentrations that are similar to or substantially higher than the comparable output of the QAC/graphite model system (Fig. 1b). This indicates that the abiotic formation of RNA within nanofluidic environments of aqueous suspensions is of general nature. Our results also imply that the output of RNA can be increased to higher concentrations by identifying appropriate particle suspension systems. The influence of the particle species on the RNA concentration, as indicated by Fig. 1b (including results from inert

polyethylene particles for comparison), is consistent with the fact that the anomalous behaviour of nanoconfined water is partly determined by the characteristics of the confining surfaces[11].

### Dynamic molecular mechanics calculations.

For nanofluidic effects to become dominant, the confining surfaces must approach, at a conservative estimate, within the range of 10 nm and below[11]. To evaluate whether stacking of nucleotides within such nanoconfinements is possible in a sufficiently stable and ordered way to prime polymerisation, we performed dynamic molecular mechanics calculations. To perform these calculations, we modelled a stack of 12 AMPs as an example system referring to the observation that polymerized AMPs of more than 10 nt length were abundant in our samples. We arranged this stack in parallel between two nanoscale separated crystals of a QAC/graphite system and added water to the confinement. Figure 4a shows the condition of the stack at the end of a dynamic simulation modelled with a confinement gap size of about 4 nm. This condition implies that the nucleotide stack remained arranged in such a confinement when surrounded by water (see also Supplementary Video 1). Comparative calculations suggest that such stacks are stable even when the density of water – which can be lower in nanoconfined conditions[11] – is decreased by approximately 60% (Fig. 4b, Supplementary Video 2). It requires a reduction of the gap size to about 3 nm and below to destabilize a stack due to increased interactions with confining surfaces (Supplementary Fig. 3). In sum, these simulations indicate that it is feasible to assume that nucleotides can associate in stable stacks within nanoconfinement gap sizes well below 10 nm for priming polymerisation.

## Discussion

Nucleotide polymerisation into RNA is a water-releasing condensation reaction that faces a thermodynamic barrier as the change in the Gibbs free energy of such a reaction is positive. Consequently, nucleotide polymerisation in water is a thermodynamically uphill reaction that is extremely inefficient to occur spontaneously under ambient conditions. However, if the entropic part ($\Delta S$) of the Gibbs free energy change ($\Delta G = \Delta H - T\,\Delta S$) becomes very positive, the reaction can become exergonic ($\Delta G < 0$) and thus favourable. As the entropic part is very positive when the activity of water is low[21] the thermodynamic barrier can be overcome by reducing water activity[25]. Against this background, we propose that our observed abiotic formation of RNA within aqueous particle suspensions can be explained by the rise of anomalous properties of water when getting temporarily confined between suspended particles: Nanoscale confinements change, among others, the vapour pressure[26] and hydrogen-bond network dynamics[11] of water. This can reduce water activity[22,26] as a function of gap size and the characteristics of the confining surfaces. We suggest that in comparison with other ways to circumvent the thermodynamic barrier of such condensation reactions, the exergonic impact of nanofluidic phenomena in aqueous particle suspensions on RNA polymerisation and stabilisation is of high relevance for prebiotic plausibility, as it does not require nonphysiological conditions such as temperatures well above 100 °C, drying events or alternative solvents.

Our results indicate that abiotic temporal nanoconfinements of water serve as natural reaction vessels for prebiotic RNA formation. The findings can solve the water paradox in such a way that nanofluidic effects in aqueous particle suspensions open up an abiotic route to biopolymerisation and polymer stabilization under chemical and thermodynamic conditions which are also prevalent within the crowded intracellular environment of living cells. The fact that polymerase enzymes also form temporal nanoconfined water clusters inside their active site[27,28] implies that the same physico-chemical effects are tapped for nucleotide condensation in water both by biochemical pathways and our reported abiotic route. These aspects indicate that our model is consistent with evolutionary conservatism stretching back to the era of prebiotic chemical evolution and the origin of cellular life[29]. The consistency is further supported by the fact that water is not trapped by nanoconfinements within the polymerase core but can exchange with the surrounding intracellular fluid[28] – a situation that also exists in abiotic nanoconfinements of water emerging temporarily between approaching particles in aqueous suspensions. Our experimental finding that under the reported conditions an amino acid catalyses the abiotic polymerisation of nucleotides may give a hint to a nanofluidic origin of cooperation between amino acids and nucleotides evolving to the interdependent synthesis of proteins and nucleic acids in living cells[30].

Abiotic RNA polymerisation in temporal nanoconfined water does not depend on highly specific mineralogical and geological environments: Now, as then in the prebiotic world, watery suspensions of micro- and nanoparticles are virtually ubiquitous[31]. They exist, for example, in the form of sediments with pore water[32], hydrothermal vent fluids containing precipitated inorganic and polyaromatic particles[33,34] or dispersed aggregates inside water-filled cracks in the crust of the earth and possibly of icy moons such as Enceladus[35].

# References


1. Benner, S. A. Paradoxes in the origin of life. *Life Evol. Biosph.***44,** 339-343 (2014).
2. Benner, S. A., Kim, H. J., Carrigan, M. A. Asphalt, water, and the prebiotic synthesis of ribose, ribonucleosides, and RNA. *Chem. Res.***45,** 2025-2034 (2012).
3. Lang, C., Lago, J., Pasek, M. A. Phosphorylation on the early earth: the role of phosphorous in biochemistry and its bioavailability. In *Handbook of Astrobiology.* (ed. Kolb, V. M.) chap. 5.8. (CRC Press, Boca Raton, Florida, 2019).
4. Yadav, M., Kumar, R., Krishnamurthy, R. Chemistry of abiotic nucleotide synthesis. *Rev.***120,** 4766–4805 (2020).
5. Marshall, M. The water paradox and the origins of life. *Nature***588,** 210-213 (2020).
6. Burton, Z. F. *Evolution Since Coding: Cradles, Halos, Barrels, and Wings* (Academic Press, San Diego, CA, 2018), p. 38.
7. Brovchenko, I., Oleinikova, A. *Interfacial and confined Water* (Elsevier, 2008), chap. 6.
8. Eijkel, J. C., Van den Berg, A. Nanofluidics: what is it and what can we expect from it? *Nanofluid.***1,** 249-267 (2005).

9. Bocquet, L., Charlaix, E. Nanofluidics, from bulk to interfaces. *Soc. Rev.***39,** 1073-1095 (2010).
10. Hart-Cooper, W. M., et al. Protein-like proton exchange in a synthetic host cavity. *PNAS***112,** 15303-15307 (2015).
11. Knight, A. W., Kalugin, N. G., Coker, E., Ilgen, A. G. Water properties under nano-scale confinement. *Rep.***9,** 1-12 (2019).
12. Reiter, G. F., et al. Evidence for an anomalous quantum state of protons in nanoconfined water. *Rev. B***85.** 045403 (2012).
13. Cafferty, B. J., Hud, N. V. Abiotic synthesis of RNA in water: a common goal of prebiotic chemistry and bottom-up synthetic biology. *Opin. Chem. Biol.***22,** 146-157 (2014).
14. Furukawa, Y. RNA synthesis before the origin of life. In *Astrobiology: From the Origins of Life to the Search for Extraterrestrial Intelligence.* (eds. Yamagishi, A., Kakegawa, T., Usui, T.) chap. 5.5. (Springer Nature, Singapore, 2019).
15. Jauker, M., Griesser, H., Richert, C. Spontaneous formation of RNA strands, peptidyl RNA, and cofactors. *Chem. Int. Ed.***54,** 14564-14569 (2015).
16. Eberle, A., Markert, T., Trixler, F. Revealing the physicochemical basis of organic solid–solid wetting deposition: Casimir-like forces, hydrophobic collapse, and the role of the zeta potential. *Am. Chem. Soc.***140,** 1327–1336 (2018).
17. Yokosawa, T., et al. A step into the RNA world: Conditional analysis of hydrogel formation of adenosine 5'-monophosphate induced by cyanuric acid. *Biosystems***162,** 53-58 (2017).
18. Norberg, J., Nilsson, L. Stacking free energy profiles for all 16 natural ribodinucleoside monophosphates in aqueous solution. *Am. Chem. Soc.***117,** 10832-10840 (1995).
19. Vernon, R. M., et al. Pi-Pi contacts are an overlooked protein feature relevant to phase separation. *Elife***7,** e31486 (2018).
20. Tribolet, R., Sigel, H. Self-association of adenosine 5'-monophosphate (5'-AMP) as a function of pH and in comparison with adenosine, 2'-AMP and 3'-AMP. *Chem.***27,** 119-130 (1987).
21. Georgelin, T., Jaber, M., Bazzi, H., Lambert, J. F. Formation of activated biomolecules by condensation on mineral surfaces–a comparison of peptide bond formation and phosphate condensation. *Life Evol. Biosph.***43,** 429-443 (2013).
22. Dass, A. V., et al. Potential role of inorganic confined environments in prebiotic phosphorylation. *Life***8,** 7 (2018).
23. Podgornik, R., Dobnikar, J. Casimir and pseudo-Casimir interactions in confined polyelectrolytes. *Chem. Phys.***115,** 1951-1959 (2001).
24. Milshteyn, D., Cooper, G., Deamer, D. Chemiosmotic energy for primitive cellular life: proton gradients are generated across lipid membranes by redox reactions coupled to meteoritic quinones. *Rep.***9,** 12447 (2019).
25. Ross, D. S., Deamer, D. Dry/wet cycling and the thermodynamics and kinetics of prebiotic polymer synthesis. *Life***6,** 28 (2016).

26. Jonchhe, S., et al. Decreased water activity in nanoconfinement contributes to the folding of G-quadruplex and i-motif structures. *PNAS***115,** 9539-9544 (2018).
27. Tropp, B. E. *Molecular Biology: Genes to Proteins*. 569-570 (Jones and Bartlett, 2008).
28. Qin, Y., et al. Direct probing of solvent accessibility and mobility at the binding interface of polymerase (Dpo4)-DNA complex. *Phys. Chem. A***117,** 13926-13934 (2013).
29. Saha, R., Pohorille, A., Chen, I. A. Molecular crowding and early evolution. *Life Evol. Biosph.***44,** 319-324 (2014).
30. Fry, I. The origin of life as an evolutionary process: Representative case studies. In *Handbook of Astrobiology* (ed. Kolb, V. M.) chap. 6.5. (CRC Press, Boca Raton, Florida, 2019).
31. Alekseyev, V. A. Nanoparticles and nanofluids in water–rock interactions. *Int.***57,** 357-368 (2019).
32. Hammond, D. Pore water chemistry. In *Marine Chemistry & Geochemistry: A Derivative of Encyclopedia of Ocean Sciences.* (eds. Steele, J. H., Thorpe, S. A., Turekian, K. K.) 2263-2271 (Academic Press, 2001).
33. Gartman, A., et al. The role of nanoparticles in mediating element deposition and transport at hydrothermal vents. *Cosmochim. Acta***261,** 113-131 (2019).
34. Konn, C., et al. Organic, gas, and element geochemistry of hydrothermal fluids of the newly discovered extensive hydrothermal area in the Wallis and Futuna region (SW Pacific), *Geofluids***2018**, 692839 (2018).
35. Postberg, F., et al. Macromolecular organic compounds from the depths of Enceladus. *Nature***558,** 564-568 (2018).
36. Determine microRNA concentration in solution: Fluorescence-based small RNA quantitation for both conventional and high-throughput assays, *BioProbes*® **70,** 32-36 (2014).
37. Garcia-Elias, A., et al. Defining quantification methods and optimizing protocols for microarray hybridization of circulating microRNAs. *Rep.***7,** 1-14 (2017).
38. Thermo Fisher Scientific Inc., “Qubit® 3.0 Fluorometer”. Publication MAN0010866. http://tools.thermofisher.com/content/sfs/manuals/qubit_3_fluorometer_man.pdf (2014).
39. Mayo, S. L., Olafson, B. D., Goddard, W. A. DREIDING: a generic force field for molecular simulations. *Phys. Chem.***94,** 8897-8909 (1990).
40. Gasteiger, J., Marsili, M. Iterative partial equalization of orbital electronegativity – a rapid access to atomic charges. *Tetrahedron***36,** 3219-3228 (1980).

# Methods

### Compounds.

Adenosine-5´-monophosphate (AMP, Sigma, disodium salt, CAS-Nr. 61-19-8); Uridine-5´-monophosphate (UMP, Alfa Aesar, disodium salt, CAS-Nr. 58-97-9); Cytidine-5´-monophosphate (CMP, Alfa Aesar, disodium salt, CAS-Nr. 6757-06-8); Guanosine-5´-monophosphate (GMP, Alfa Aeasar, disodium salt, CAS-Nr. 85-32-

5); L-Arginine (Alfa Aesar, CAS-Nr. 74-79-3); Quinacridone (Clariant GmbH, CAS-Nr. 1047-16-1); Anthraquinone (Fluka, CAS-Nr. 84-65-1); carbon nanopowder (<50 nm (TEM); Sigma Aldrich, CAS-Nr. 7440-44-0); Carbon (mesoporous, Sigma Aldrich, CAS-Nr. 1333-86-4); Iron (II, III) oxide (Sigma Aldrich, CAS-Nr. 1317-61-9); Silicon dioxide (-325mesh, Sigma Aldrich, CAS-Nr. 60676-86-0); Polyethylene (<400 micron, Alfa Aesar, CAS-Nr.9002-88-4).

### Suspension preparation.

Three millilitre of aqueous suspension was made of each 0.1 g/ml inorganic substrate (e.g., graphite powder) and/or organic pigment with a total nucleoside monophosphate concentration of 50 mM. Samples were incubated overnight at 60°C while mixed horizontally at 300 rpm, to avoid sedimentation of substrates and pigment. After incubation, samples were centrifuged at 8000x g for 1 min at room temperature (RT). The supernatant was transferred to a new collection tube.

### Precipitation.

Precipitation was carried out with 0.2 M NaCl and 3.5 volumes of EtOH for isolation of short RNAs (2–10 nt), and with 0.3 M NaOAc (pH 5.2) and 0.7 volumes of isopropanol for isolation of longer RNAs (> 10 nt). After the addition of the appropriate amount of salt solution and alcohol, samples were mixed by inverting the tubes 5 times, and precipitation reactions were incubated overnight at -20°C. Afterwards the samples were subsequently centrifuged at 14.000x g, for 1 hour at room temperature. The supernatant was discarded, leaving approximately 20 µl of it inside the reaction tube, in addition to any formed gel pellet. Formed gel pellets were dried at 37°C for 20 min and resuspended in an appropriate amount of $H_2O$ dest.

### Concentration measurements.

Concentrations of miRNA suspensions were measured using a Qubit® 3 Fluorometer (Invitrogen™), the Qubit® microRNA Assay Kit (Invitrogen™) or the Qubit® RNA HS Assay Kit (Invitrogen™)[36] due to its high specificity and reliability[37]. Concentrations were calculated by the chosen miRNA or RNA program of the Qubit® 3 Fluorometer. Standard curves and samples were prepared following the manuals[38]. Concentrations were calculated and normalized regarding the respective volume of each sample.

### Quantitative RT-qPCR.

For RT-qPCR, selected samples were reverse transcribed using the TaqMan™ Advanced miRNA cDNA Synthesis Kit (Thermo Fisher) following the manual. As a positive control, the synthetic miRNA hsa-miR-134-3p (5´-phosphorylated) (eurofins) with an oligonucleotide length of 23 nt was used. As a negative control nuclease-free water was used. For qPCR, the Master Mix reaction was composed of 10 µl QuantiTect SYBR® Green (Qiagen), 2 µl amplification primer mix from the TaqMan™ Advanced miRNA cDNA Synthesis Kit (Thermo Fisher), and 8 µl of diluted sample. qPCR was ran on a LightCycler® 480

Instrument II with the following settings: 15min 95°C, 40x: 15s 94°C – 30s 60°C – 30s 72°C – Single Data Acquisition, 72°C 2 min, Melting curve.

### Scanning tunnelling microscopy.

For scanning tunnelling microscopy (STM) investigations aqueous suspensions were prepared of each 2% w/w quinacridone pigment and a nucleotide monophosphate or amino acid final total concentration of 25 mM, if required. Suspensions were drop cast onto graphite substrates to induce OSWD[16] and dried overnight. The samples were subsequently covered with dodecane to achieve a defined, stable environment between the STM tip and substrate. Each sample was prepared twice. From each replicate, 15 images of 200 nm x 200 nm size were generated from 3 different spots. Images were acquired with a self-built STM combined with an *SPM 100* control system supplied by *RHK Technology*. The scan settings were: bias = 1 V, tunnel current = 300 pA, and line time = 50 ms. Further, the voltage pulses used to improve the scan quality were applied within the range of 4.3 V to 10 V. All STM measurements were performed under ambient conditions.

### Surface coverage determination.

To determine coverage, meaning how much area of graphite is covered by supramolecular QAC adsorbate structures (Supplementary Fig. 1), black/white histograms were created. For this purpose, depicted QAC adsorbate structures were masked out in the image (white) while setting the background (graphite without QAC adsorbate structures) to black (Supplementary Fig. 2). Black/white histogram values were calculated using "*histogram*" within the "*analyse*" menu of the software ImageJ. The mean values given in the histogram data box were then converted to percentages of the graphite area covered with QAC adsorbate structures, whereby a histogram value of 0 means 0% of the graphite surface is covered with adsorbate and a histogram value of 255 means 100% of the graphite surface is covered. Note that AMP itself does not form monolayers on graphite due to its 3D-structure. For statistical analysis of the coverage results, a t-test with Welch's corrections was used since the samples show unequal distribution variance. The calculations were performed using Excel, giving the results of a two sided unequal variance t-test.

### Computer simulations.

All molecular mechanics calculations were performed with the Materials Studio package (*Accelrys*). The force field used was Dreiding[39], where partial charges of atoms within the molecule are calculated with the Gasteiger method[40]. Geometry optimisation calculations were calculated where convergence tolerance regarding energy was 1.0e-4 kcal/mol, force was 0.005 kcal/mol/Å and displacement was 5.0e-5 Å. The Smart algorithm was used which is a concatenation of steepest descent, Newton-Raphson and quasi-Newton methods, to obtain better behaviour for the different stages of downstream minimization. Dynamic calculations were performed for an NVE ensemble with a temperature of 298 K, random values assigned for the initial velocities of the atoms and a time step of 0.1 fs for the integration algorithm.

A chain of 12 AMP molecules was constructed starting with building an AMP dimer. The dimer itself was built by duplicating an AMP and performing a 180° rotation related to the axis lying in the plane of the adenine molecule and passing through the centres of the hexagon and pentagon. Afterwards, the rotated AMP was translated normal to the plane of the adenine by a distance of 3.5 Å. This dimer was stacked 6 times in a row such that all planes of the adenine molecules were parallel each by a distance of 3.5 Å. This artificially constructed model was finally optimized related to geometry.

The entire system is modelled within a supercell containing two graphene layers, on top at some distance a chain of AMP molecules and finally two layers of a QAC crystal above the AMP chain. The entire system was filled with water molecules at different concentrations. The initial position of the AMP chain related to the graphene layers and the QAC crystal layers is stated below for the different calculations performed. The vertical dimension of the supercell has been chosen to be safe so that an interaction of the graphene layers and the QAC crystal layers can be neglected (gap is 43 Å). The rectangular in-plane dimensions of the supercell have been determined to minimize the distortion of the periodic structure of the QAC crystal layers. The deviation of the unit cell vectors of the QAC layers is almost zero in one direction (0.1%) but quite large in the other direction (5.6%). However, because the outer layer of the QAC crystal is always kept fixed, the adjacent free movable QAC layer was observed to be stable throughout all simulations. This observation was the reason why this significant deviation was accepted for all calculations. The graphene layers are not distorted with regard to the optimal unit cell dimensions. The dimensions of the supercell are: plane x, y: 80.956 Å, 56.58 Å, and z: 103.4 Å.

# Declarations


### Acknowledgments

We thank J. Herms and F. Strübing for technical and practical support regarding qPCR and RNA concentration measurements at the Center for Neuropathology and Prion Research, LMU, Germany. F.T. has received funding from the Bavarian State Ministry of the Environment and Consumer Protection grant agreement no. 71k-U8793-2015/14-9. This work was supported by the mentoring program of the Nanosystems Initiative Munich (NIM).


### Author contributions

A.G.H. designed and performed experiments and data analysis, T.M. designed and performed computer simulations, F.T. conceived the project and directed the research, F.T. and A.G.H. wrote the manuscript.

### Competing interests

The authors have no competing interests.

### Additional Information

Supplementary information is available for this paper.

Correspondence and requests for materials should be addressed to F.T.

# Figures

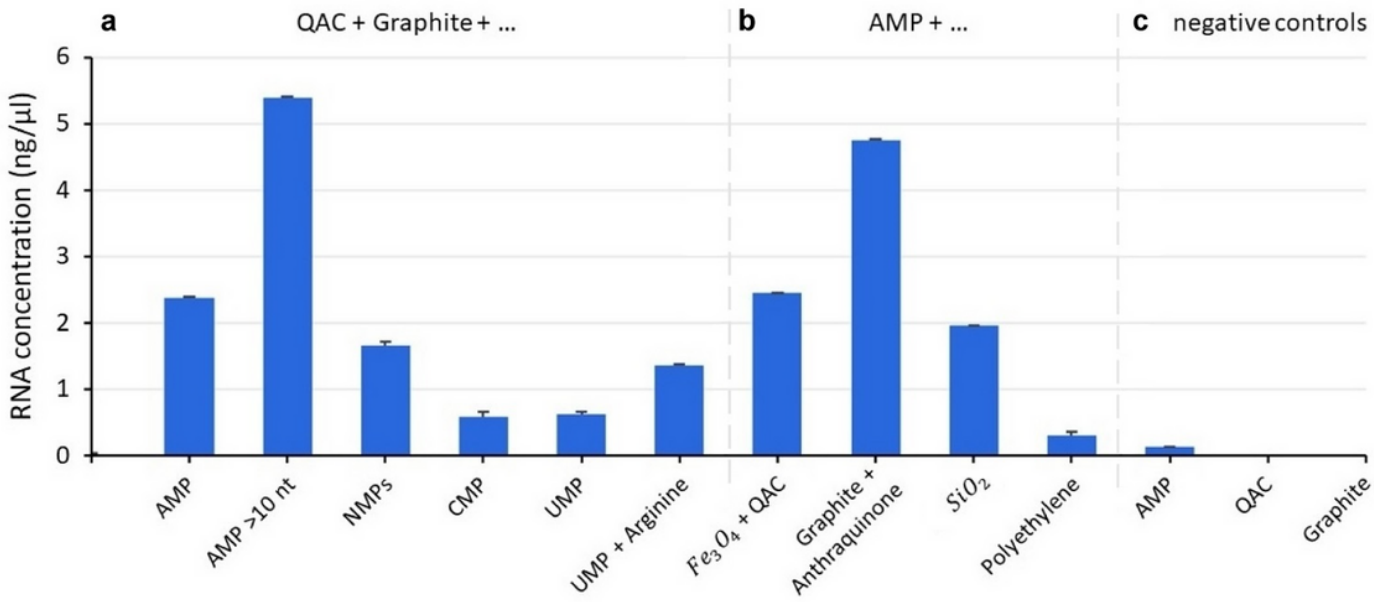


**Figure 1**

Fluorometric results of RNA concentration measurements in aqueous particle suspensions. Displayed are the mean values of three measurement replicates and standard deviations. If not differently indicated, nucleotide suspensions had a final concentration of 50 mM. RNA isolation was performed from aqueous suspensions of particles containing dissolved biomolecules. a, Detected RNA concentrations in samples based on QAC + graphite suspensions: AMP: 2.38 ng/µl; AMP > 10 nt: 5.4 ng/µl; mixture of NMPs (AMP, UMP, GMP, CMP, 12.5 mM each): 1.66 ng/µl; CMP: 0.59 ng/µl; UMP: 0.62 ng/µl; mixture of UMP and arginine: 1.36 ng/µl. b, Detected poly-A-RNA concentrations in suspensions based on: Fe3O4/QAC: 2.45 ng/µl; graphite/anthraquinone: 4.76 ng/µl; SiO2: 1.96 ng/µl; polyethylene: 0.3 ng/µl. c, Results of the negative controls: aqueous samples containing AMP but without suspended particles: 0.14 ng/µl; pure aqueous samples only containing QAC or graphite: both underneath the detection level.

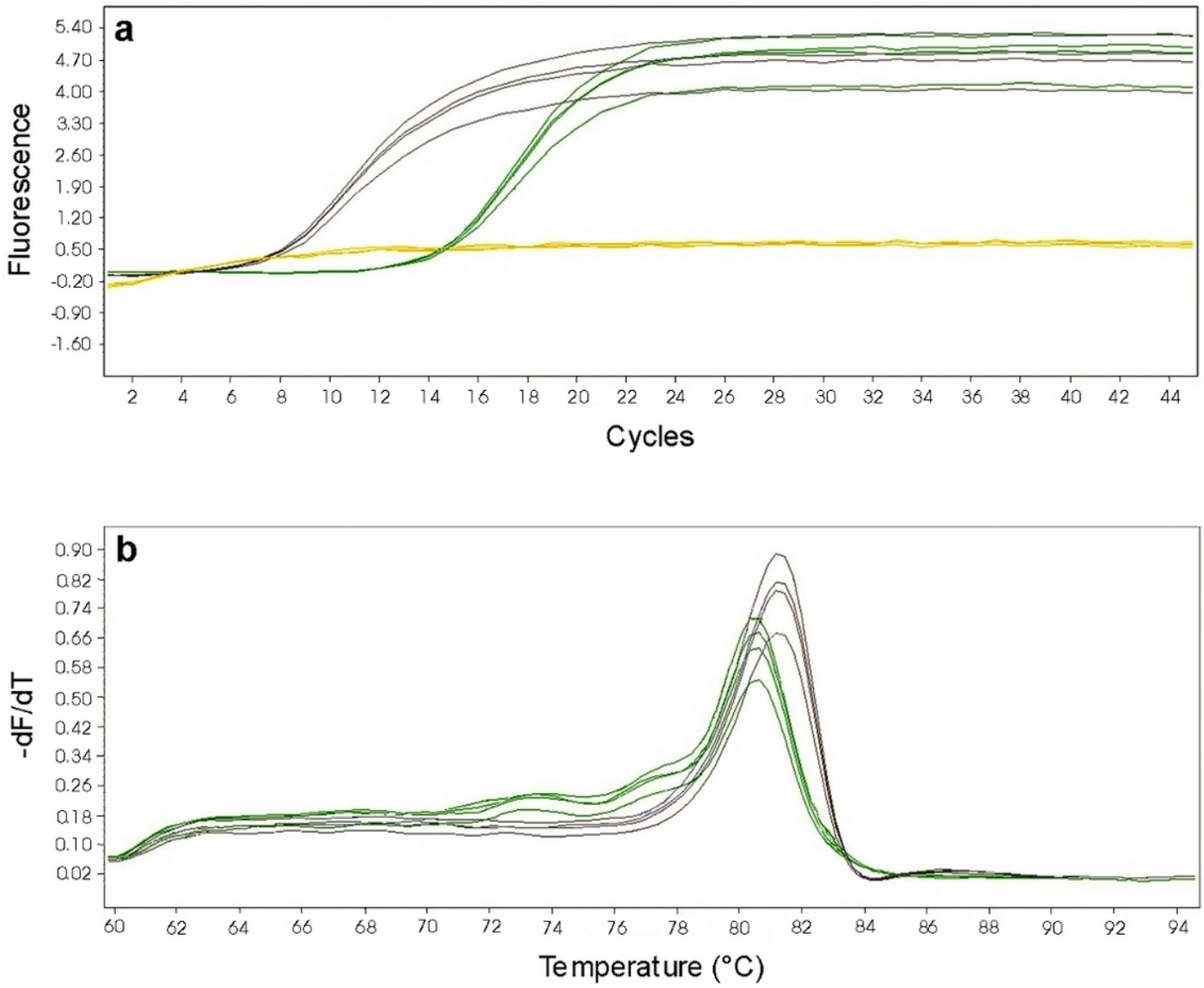


## Figure 2

Quantitative PCR after reverse transcription (RT-qPCR) applied to an aqueous particle suspension with dissolved AMP. Yellow: negative control; green: positive control (synthetic miRNA hsa-miR-134-3p (5´-phosphorylated)); black: sample (precipitation from sample “QAC + Graphite + AMP”, Fig. 1a). a, Fluorescent signals of qPCR. The signals exceed the background fluorescence (yellow) after 7.57 cycles (sample) and 14.25 cycles (positive control). b, Melting curves. Medium melting point: positive control (green): 80.53 °C, sample (black): 81.31 °C.

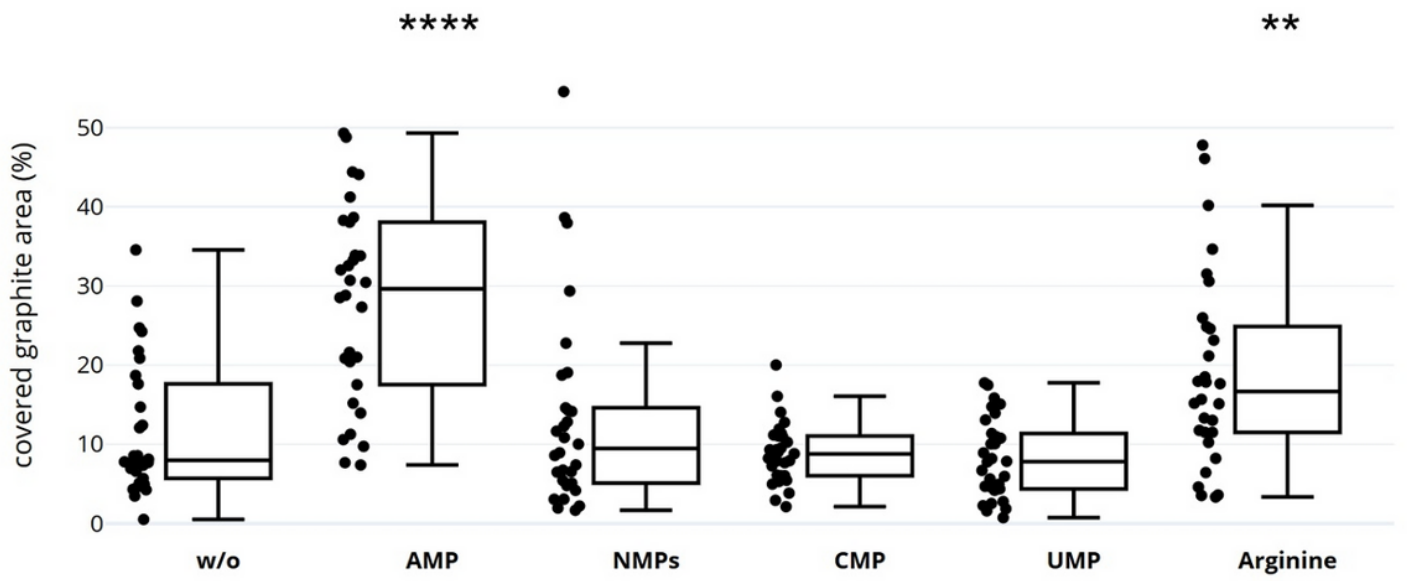


## Figure 3

OSWD efficiency as a function of biomolecular species added to aqueous particle suspensions. The box plots and distributions of values are based on results obtained by STM. The statistical analysis of the results reveals the coverage of graphite surfaces with QAC adsorbates. The adsorbate forms after graphite has been brought into contact with a watery suspension of QAC particles that either contains dissolved biomolecules (AMP, NMPs, CMP, UMP, arginine) or no biomolecules (w/o). Testing: t-test with Welch´s correction; n=30; **: p<0.01; ****: p< 0.0001.

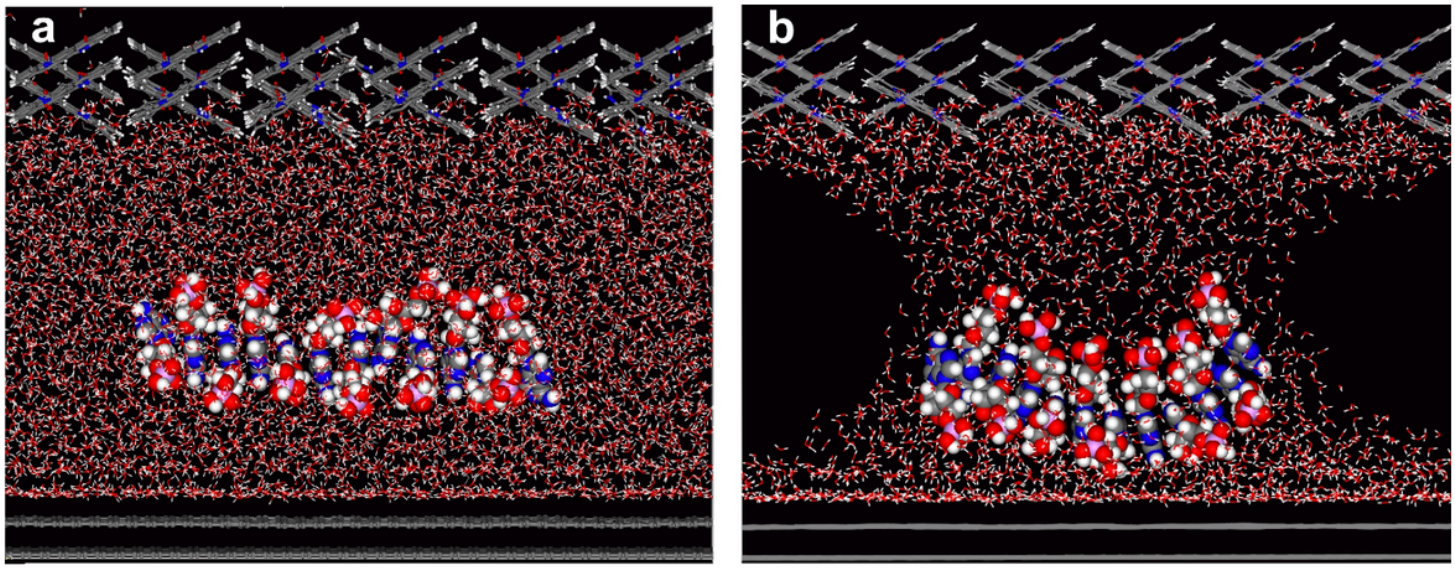


## Figure 4

Dynamic force field calculation of a nucleotide stack in nanoconfined water. The system is modelled within a supercell containing two graphene layers (bottom), two layers of a QAC crystal (top) and a stack

of 12 AMP molecules placed between the confining surfaces. Vertical dimension of the gap: 43 Å. a, Condition of the stack after a simulated time span of 50 ps. The confinement is filled with water molecules. b, Condition of the stack after a simulated time span of 60 ps and a water density of approximately 60%.

## Supplementary Files

This is a list of supplementary files associated with this preprint. Click to download.

- SupplementaryVideo1.mp4
- SupplementaryVideo2.mp4
- SupplementaryInformationGreinerMarkertTrixler.docx